

Contribution of Molecular Modeling and Site-Directed Mutagenesis to the Identification of a New Residue, Glutamate 215, Involved in the Exopeptidase Specificity of Aminopeptidase A[†]

Raphaël Rozenfeld,[‡] Xavier Iturriz,^{‡,§} Mayumi Okada,[‡] Bernard Maignet,^{||} and Catherine Llorens-Cortes^{*,‡}

INSERM Unité 36, Collège de France, 11, place Marcelin Berthelot, 75005 Paris, France, and CNRS, Unité Mixte de Recherche 7565, Laboratoire de chimie théorique, Université de Nancy, 54506 Vandoeuvre les Nancy, France

Received March 5, 2003; Revised Manuscript Received October 17, 2003

ABSTRACT: Aminopeptidase A is a zinc metalloenzyme that generates brain angiotensin III, which exerts a tonic stimulatory action on blood pressure in hypertensive animals. We have previously constructed a three-dimensional model of the ectodomain of this enzyme, using the crystal structure of leukotriene A4 hydrolase/aminopeptidase as a template. According to this model, Glu-215, which is located in the active site, hydrogen bonds to the amino moiety of the inhibitor, 4-amino-4-phosphonobutyric acid (GluPhos), a phosphonic acid analogue of glutamic acid. Replacement of this residue with an aspartate or an alanine in the model abolished this interaction and led to a change in the position of the inhibitor in the active site. Mutagenic replacement of Glu-215 with an aspartate or an alanine drastically reduced the affinity of the recombinant enzymes for the substrate by a factor of 10 or 17, respectively, and the rate of hydrolysis by a factor of 14 or 6, respectively. Two isomers of GluPhos with different N-terminal amine positions differed considerably in their ability to inhibit the wild type (by a factor of 40), but not the mutated enzymes. These results, together with the interaction predicted by the model, demonstrate that Glu-215 interacts with the N-terminal amine of the substrate, thereby contributing, together with Glu-352, to the determination of the exopeptidase specificity of aminopeptidase A.

Aminopeptidase A (APA,¹ EC 3.4.11.7) is a 160 kDa homodimeric type II membrane-bound zinc aminopeptidase that specifically cleaves the N-terminal glutamyl or aspartyl residue from peptide substrates such as angiotensin II (AngII) and cholecystokinin-8 *in vitro* (1, 2). APA is present in many tissues, particularly in the brush border of intestinal and renal epithelial cells and in the vascular endothelium (3). APA and other components of the brain renin–angiotensin system (4) have been identified in several brain nuclei involved in the control of body fluid homeostasis and cardiovascular functions. Studies with specific and selective APA inhibitors (5) have shown that *in vivo* APA converts brain AngII to angiotensin III (AngIII) (6) and that brain AngIII exerts a tonic stimulatory action on the central control of blood pressure in hypertensive animals (7). The central administration of APA inhibitors results in a large decrease in arterial blood pressure in alert spontaneously hypertensive rats (7),

suggesting that brain APA is a putative central therapeutic target for the treatment of hypertension (reviewed in ref 8). In the absence of data concerning the structure of monozinc aminopeptidases, site-directed mutagenesis studies based on alignment of the sequence of APA with those of other monozinc aminopeptidases were initially used to probe the organization of the APA active site (9–14). On the basis of the functional data collected in these studies, and the recently determined X-ray crystal structure of leukotriene A4 hydrolase (LTA4H, EC 3.3.2.6) (15), a bifunctional zinc metalloenzyme with both epoxide hydrolase and aminopeptidase activities, we constructed a three-dimensional (3D) model of the mouse APA ectodomain from residue 79 to 559 (16). This model predicts that APA is folded into a flat triangle composed of three different domains: the N-terminal domain consisting mainly of β -sheets, the globular active site domain, and the C-terminal helical domain. In the 3D model of APA, the zinc atom is coordinated by the two histidine residues (His-385 and His-389) of the HEXXH motif, consistent with the results obtained by Wang and Cooper (9). The zinc atom is also coordinated by a water molecule and Glu-408, which was shown by Vazeux *et al.* to be the third zinc ligand (10). We then docked a potent and selective APA inhibitor, 4-amino-4 phosphonobutyric acid (GluPhos), a phosphonic acid analogue of glutamic acid, into the active site. It has been suggested that this compound binds to APA by interacting with the S1 subsite specific for N-terminal acidic residues. This inhibitor behaves as a transition state analogue in which replacement of the substrate scissile peptide bond

[†] We thank the CINES for a computing grant. M.O. was supported by la Fondation pour la Recherche Médicale.

* To whom correspondence should be addressed: INSERM Unité 36, Collège de France, 11, place Marcelin Berthelot, 75005 Paris, France. Telephone: (331) 44.27.16.63. Fax: (331) 44.27.16.91. E-mail: c.llorens-cortes@college-de-france.fr.

[‡] Collège de France.

[§] Present address: Protein Phosphorylation Laboratory, Cancer Research UK London Institute, Lincoln's Inn Fields Laboratories, 44 Lincoln's Inn Fields, London WC2A 3PX, U.K.

^{||} Université de Nancy.

¹ Abbreviations: APA, aminopeptidase A; AngII, angiotensin II; AngIII, angiotensin III; APN, aminopeptidase N; LTA4H, leukotriene A4 hydrolase; 3D, three-dimensional; MD, molecular dynamics; GluNA, α -L-glutamyl- β -naphthylamide; RMS, residual-mean-square.

with a phosphonic acid group mimics the tetrahedral transition state (17), with one of its phosphoryl oxygens ligating the zinc in a tetrahedral complex and another one hydrogen bonding with Tyr-471 which is involved in transition state stabilization (11). The 3D model of APA complexed with GluPhos also provides evidence that the N-terminal amine of the inhibitor interacts with the Glu-352 residue of APA. The role of this glutamate, located in the conserved GXMEN motif, has been extensively studied in several aminopeptidases by site-directed mutagenesis (12, 18). These studies demonstrated the requirement for a binding site for the N-terminus of the substrate of monozinc aminopeptidases, being responsible for the exopeptidase specificity. A similar interaction has been observed between Glu-271 of LTA4H and the N-terminal amine of the cocrystallized inhibitor bestatin (15). The involvement of this residue in the binding site for the N-terminus of the substrate was confirmed by site-directed mutagenesis (19). Interestingly, the three-dimensional model of the active site of APA showed that a second residue interacts with the N-terminal amine of the inhibitor GluPhos. This residue, Glu-215, is located in the active site, within the loop of residues 215–230, which has been shown to be critical for protein structure and activity (16). In the model, Glu-215 interacts with the N-terminal amine of the inhibitor via two hydrogen bonds between the oxygens of the acidic function of the lateral chain of the residue and the free amino group of the inhibitor. Thus, Glu-215 together with Glu-352 may be involved in determining the exopeptidase specificity of APA. We used site-directed mutagenesis to confirm the functional role of Glu-215. We replaced Glu-215 with a glutamine, an aspartate, and an alanine. We first ensured that the mutated enzymes displayed maturation and subcellular localization similar to those of wild-type APA. We then studied the enzymatic activity of the recombinant wild-type and mutated purified APAs, and followed in parallel the effects of the mutations on the 3D model of APA.

EXPERIMENTAL PROCEDURES

Materials

Restriction endonucleases and DNA-modifying enzymes were obtained from New England Biolabs (Hitchin, England) and were used according to the manufacturer's instructions. The Expand high-fidelity Taq polymerase PCR system was purchased from Roche Molecular Biochemicals (Mannheim, Germany). The liposomal transfection reagent, Lipofect-AMINE 2000, the pcDNA 3.1-His vector, and the anti-Xpress antibody were purchased from Invitrogen (Groningen, The Netherlands). The anti-His₅ antibody was purchased from QIAGEN Inc. The alkaline phosphatase-conjugated goat anti-mouse antibody was purchased from Immunotech. Immobilized cobalt affinity columns (Talon) were obtained from CLONTECH (Heidelberg, Germany). The synthetic substrate α -L-glutamyl- β -naphthylamide (GluNA) was purchased from Bachem (Bubendorf, Switzerland). The inhibitors methylphosphonic acid (methylPhos) and (aminomethyl)-phosphonic acid (GlyPhos) were purchased from Sigma-Aldrich (Schnelldorf, Germany).

Methods

Modeling of APA. The model of the complex between GluPhos and the wild-type enzyme used here was the one described previously (16). We summarize only briefly here the main steps of this modeling procedure. We constructed a 3D homology model, using the X-ray crystallographic structure of human LTA4H (15) as the template. The model was completed by adding the missing loops connecting the moieties obtained by coordinate transfer. The APA model obtained therefore included only residues 79–559, which is the region most highly conserved between APA and LTA4H (31% similarity).

This model was next placed within a 85 Å³ water box and subjected to a refinement procedure, including several rounds of energy minimization (until convergence) and short molecular dynamics (MD) runs (100 ps at 300 K). This process was carried out to check the stability of the model over time.

We carried out docking calculations, using as the ligand the selective APA inhibitor GluPhos. This inhibitor was introduced according to the position of bestatin in LTA4H. Our modeling studies were performed considering the following ionization states for the ionizable chemical groups in the protein: all the carboxyl groups were anionic, and the ammonium groups were cationic as were the guanidinium ones. In the GluPhos inhibitor, we have considered ionic phosphate and carboxylate groups. A Zn²⁺ metal was considered. However, there are some questions regarding the ionization state of the GluPhos amine group and of the surrounding Glu-215 and Glu-352 side chains. According to the available data about the monozinc aminopeptidase catalytic mechanism (18, 19), we postulate that the Glu-352 side chain is in a carboxylate ionic form. With respect to the GluPhos amine and the Glu-215 moieties, these groups may be in the zwitterionic form with an ammonium and a carboxylate, or in a neutral state with an NH₂ group on the ligand and a COOH group on the Glu-215 side chain. To answer to this question, we performed preliminary QM calculations using the AM1 semiempirical method (20) on a model system of the APA catalytic site. Our calculations are in favor of the neutral form (not shown), in good agreement with *ab initio* results on the trimethylamine–formic acid system (21). We assumed, therefore, that Glu-215 and the amine nitrogen group of GluPhos are not ionic. Thus, in all our calculations, the nitrogen atom of GluPhos should not be considered ionic, nor should the Glu-215 residue. The system protein–ligand–solvent box was relaxed step by step, until all the degrees of freedom were considered in the minimization and MD processes. After several steps of energy minimization, 100 ps of MD, and energy minimization, the model was considered to be stable as the residual-mean-square (rms) deviations between the C α atoms of the starting structure and the final structure were less than 1.

In this paper, the models of the complexes between GluPhos and the APA mutants were constructed according to the following steps.

(1) First, the concerned mutated residues were changed within the wild-type APA model described above using the InsightII/Biopolymer/Residue/Replace command.

(2) Next, after a preliminary short minimization round keeping everything fixed in the complex except the mutated residue, all protein side chains were unconstrained as well as the inhibitor, and another minimization round was performed until convergence of the conjugate gradient process.

(3) Finally, for each mutant complex, everything was relaxed and minimized, a short MD run of 100 ps performed, and a final minimization round performed. We considered that, starting from a stable wild-type model to build each mutant, several rounds of energy minimization, 100 ps of MD, and energy minimization were not necessary to achieve a stable state compared to what was done for the previous wild-type modeling (16). This was assessed by checking that the $\langle \text{rmsd} \rangle$ between all heavy atoms was kept below 2.0 Å during this procedure.

(4) The final models were the ones used for discussion.

All preliminary calculations were carried out on SGI O2 workstations, and the heaviest calculations were performed at the CINES supercomputing center, on an Origin 3800 computer.

Cloning and Site-Directed Mutagenesis. The mouse cDNA encoding APA was inserted into the expression vector pcDNA 3.1 His (13), and mutants were generated by PCR-based site-directed mutagenesis, as previously described (22). Two overlapping regions of the cDNA were amplified separately, using two flanking oligonucleotides: A (5'-TTAATACGACTCACTATAGGGA-3', positions 862–883) as a forward primer and B (5'-GAATCCTAAGATAGAG-GCCCGGAG-3', positions 3215–3238) as a reverse primer and two overlapping oligonucleotides at positions 1553–1576 containing the mutated residues (C1D1 for Gln-215, C2D2 for Asp-215, and C3D3 for Ala-215): forward primers, 5'-CACTGACCATCAACCAACAGATG-3' (C1), 5'-CACTGACCATGATCCAAACAGATG-3' (C2), and 5'-CACTGACCATGCACCAACAGATG-3' (C3); and reverse primers, 5'-CATCTGTTGGTTGATGGTCAGTG-3' (D1), 5'-CATCTGTTGATCGATGGTCAGTG-3' (D2), and 5'-CATCTGTTGTGCGATGGTCAGTG-3' (D3). The underlined bases encode the new amino acid residue replacing glutamate at position 215. Nucleotides are numbered according to the mouse APA sequence (23) deposited in the GenBank (entry M29961).

The products of the first two rounds of amplification (A–D_{1–3} and B–C_{1–3}) were used as the template for a second PCR with the two flanking oligonucleotides, A and B. For all PCRs, high-fidelity Taq polymerase (Roche) (1 unit) was used (25 cycles at 94 °C for 30 s, 54 °C for 45 s, and 72 °C for 2 min). The final 2376 bp PCR product was digested with *Hind*III and *Eco*RV (New England Biolabs), and the resulting 1505 bp *Hind*III–*Eco*RV fragment containing the mutation was used to replace the corresponding nonmutated region (*Hind*III–*Eco*RV) of full-length APA cDNA. The presence of the mutation and the absence of nonspecific mutations were confirmed by automated sequencing on an Applied Biosystems 377 DNA sequencer with dye deoxy-terminator chemistry.

Cell Culture, Establishment of Stable CHO-K1 Cell Lines Producing Wild-Type and Mutated His₆-APAs, and Purification of Recombinant His₆-APA. CHO-K1 (American Type Culture Collection, Rockville, MD) cells were maintained in Ham's F12 medium supplemented with 7% fetal calf

serum, 0.5 mM glutamine, 100 units/mL penicillin, and 100 µg/mL streptomycin (all from Boehringer-Mannheim, Mannheim, Germany). Cells were transfected with 1 µg of plasmid containing the wild-type or mutated His₆-APA cDNA, using a liposomal transfection reagent (LipofectAMINE 2000), and stable cell lines producing the polyhistidine-tagged wild-type and mutated APA were established as previously described (13). As previously described (13), stably transfected CHO cells were harvested and a crude membrane preparation was obtained. Wild-type and mutated His₆-APA were purified from the solubilized crude membrane preparation by metal affinity chromatography with a metal chelate resin column (Talon Co²⁺), as previously described (13). The purity of the final preparation was assessed by SDS–polyacrylamide gel electrophoresis (PAGE) in 7.5% polyacrylamide gels, as described by Laemmli (24). Proteins were stained with Coomassie Brilliant Blue R-250. Protein concentrations were determined by the Bradford assay (25), using bovine serum albumin (BSA) as the standard. We systematically verified that the protein concentration estimated by the Bradford assay for the various recombinant His₆-APA reflected the true concentration of APA. We used dot blots of recombinant purified His₆-APA for this purpose. A standard curve was generated by spotting various amounts of purified wild-type His₆-APA onto a nitrocellulose membrane. Dot blots of recombinant purified His₆-APAs were probed with a monoclonal anti-Xpress antibody (1:5000 dilution). Immunoreactive material was detected with an alkaline phosphatase-conjugated goat anti-mouse antibody (1:7000). Alkaline phosphatase activity was detected with the AttoPhos AP Fluorescent Substrate System (Promega, Madison, WI). Membrane fluorescence was analyzed with a Molecular Imager FX Proplus, and quantified with Quantity One software (Bio-Rad, Hercules, CA). The concentrations of the purified mutant His₆-APAs were calculated from the purified His₆-APA standard curve.

Metabolic Labeling and Immunoprecipitation. Stably transfected CHO cells producing wild-type and mutated His₆-APA were incubated for 5 h in a methionine/cysteine serum-free medium (Ham's 12) supplemented with 100 µCi/mL of [³⁵S]methionine/cysteine. The cell medium was discarded, and the cells were harvested and proteins solubilized by incubation overnight at 4 °C with 500 µL of 50 mM Tris-HCl buffer (pH 7.4), 150 mM NaCl, 10 mM EDTA, and 1% (v/v) Triton X-100. The resulting lysate was centrifuged at 20000g for 10 min at 4 °C to remove insoluble material. The supernatant was incubated with monoclonal mouse anti-His₅ antibody (Qiagen) (5 µL, 1 µg) and protein A–Sepharose (Pharmacia-LKB Biotechnology) [50% (w/v) suspension in solubilization buffer] for 2 h at 4 °C for immunoprecipitation. The immune complexes were collected by centrifugation and washed four times with the solubilization buffer and once with 20 mM Tris-HCl buffer (pH 6.8). Proteins were eluted by being boiled in 25 µL of Laemmli buffer and resolved by 5% SDS–PAGE. The gel was dried and analyzed with a Molecular Imager FX Proplus machine (Bio-Rad).

Immunofluorescence of Stably Transfected CHO Cells. CHO cells producing wild-type and mutated His₆-APAs were dispensed (25 000 cells) on 14 mm diameter coverslips. The cells were cultured for 24 h in Ham's F12 medium in a humidified atmosphere of 5% CO₂ and 95% air. They were then incubated with cycloheximide (70 µM) in Ham's F12

medium for 90 min, fixed, and permeabilized by incubation for 5 min in 100% ice-cold methanol. The cells were rinsed three times in 0.1 M phosphate-buffered saline (PBS, pH 7.4), and then saturated by incubation with 5% BSA for 30 min at room temperature (RT). They were then incubated with a 1:500 dilution of rabbit polyclonal anti-(rat APA) serum (26) in 2% BSA in PBS, for 2 h at RT. The coverslips were washed three times with cold PBS and then incubated with a 1:500 dilution of cyanin 3-conjugated polyclonal anti-rabbit antibody in 2% BSA in PBS for 2 h at RT. The coverslips were washed four times with PBS and mounted in Mowiol (Sigma-Aldrich) for confocal microscopy. Cells were examined with a Leica TCS SP II (Leica Microsystems, Heidelberg, Germany) confocal laser scanning microscope equipped with an argon/krypton laser and configured with a Leica DM IRBE inverted microscope. Cyanin 3 fluorescence was detected after 100% excitation at 568 nm. Images (1024×1024 pixels) were obtained with a $63\times$ magnification oil-immersion objective. Each image corresponded to a cross section of the cell.

Enzyme Assay. The enzymatic activities of the wild-type and mutated His₆-APAs were determined in a microtiter plate, by monitoring the rate of hydrolysis of a synthetic substrate, α -L-glutamyl- β -naphthylamide (GluNA), as previously described (27). Purified wild-type and mutated recombinant His₆-APAs were incubated at 37 °C in the presence of various concentrations of GluNA, with 4 mM CaCl₂, in a final volume of 100 μ L of 50 mM Tris-HCl buffer (pH 7.4).

The kinetic parameters (K_m and k_{cat}) were determined from Lineweaver–Burk plots with a final concentration of GluNA of 0.025–2 mM. All enzymatic assays were performed under initial velocity conditions. Spontaneous hydrolysis of the substrate was corrected by subtracting the absorbance of blank incubations without enzyme. The sensitivity of wild-type and mutated His₆-APAs to inhibition by glutamate thiol [D,L-GluSH (28)], glutamate phosphonic acid [L-GluPhos and D-GluPhos (17)], glycine phosphonic acid (D,L-GlyPhos), and methylphosphonic acid (methylPhos) was determined by establishing dose-dependent inhibition curves for a final GluNA concentration of 0.5 mM and calculating K_i values with Graph Pad Prism 2 software. Statistical comparisons were performed with a Student's unpaired *t* test. Differences were considered significant if *p* was less than 0.05.

RESULTS

Modeling of APA. The modeling of APA residues 79–559 showed the protein to be organized into three domains: the N-terminal domain consisting mostly of β -sheets, the globular active site domain, and the C-terminal helical domain. The N-terminal and C-terminal domains have a large interface in common. The active site was found to be located in the middle of this interface and to be accessible from the outside.

The APA active site structure obtained in the presence of the inhibitor GluPhos is presented in Figure 1. The Zn²⁺ ion is hexacoordinated in the model by (1) the three active site residues His-386, His-389, and Glu-408 and (2) one of the oxygen atoms of the phosphate of the inhibitor and a water molecule from the solvent.

A strong network of hydrogen bonds is kept stable during the dynamics around the zinc coordination sphere: the water

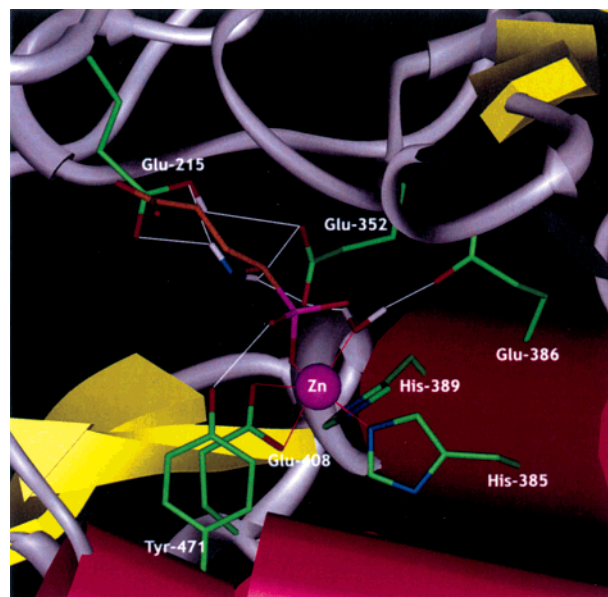


FIGURE 1: Structure of the GluPhos–wild-type APA complex. The zinc atom is shown as a purple sphere. The carbon atoms of the active site residues are depicted in green. The carbon atoms of the inhibitor GluPhos are depicted in brown. The Zn–ligand interactions are shown as red lines; the hydrogen bonds between the active site residues and between the inhibitor and the active site residues are shown as white lines.

molecule bound to the zinc ion being frozen in a stable position as it is also engaged in two conserved hydrogen bonds with the Glu-386 and Glu-352 side chains. The Glu-352 and Glu-215 side chains are also hydrogen-bonded to the amine moiety of the inhibitor. The interaction between Glu-215 and the inhibitor appears to be important for the positioning of the inhibitor in the active site. This residue is not strictly conserved among monozinc aminopeptidases. The corresponding residues in the other known enzymes (Figure 2) are glutamates [in mouse puromycin-sensitive aminopeptidase (EC 3.4.11.14), rat insulin-stimulated aminopeptidase (EC 3.4.11.3), and rat LTA4H] or glutamines [in mouse, rat, and human APN, mouse and human LTA4H, and rat aminopeptidase B (EC 3.4.11.6)]. If Glu-215 is replaced with an alanine, an aspartate, or a glutamine in the model, and 100 ps of molecular dynamics simulations are run on the new system, the organization of the active site is not disrupted, at least for the zinc ligands, while local differences are observed for other moieties. Figure 3 shows the active sites of wild-type APA and the Gln-215, Asp-215, and Ala-215 mutants, with the inhibitor GluPhos docked into the active site, and a superimposition of the three models. In the model of the Gln-215 mutant, the carbonyl group of the amide function of Gln-215 is hydrogen-bonded to the N-terminal amine moiety of the inhibitor. Gln-215 also interacts with Glu-352, stabilizing this residue in a position slightly different from that of the wild type. This change in position involves a shortening of the hydrogen bond between Glu-352 and the water molecule (from 1.74 Å in the wild type to 1.63 Å in the mutant), and a slight shift in the position of the water molecule, which interacts with Glu-386 via a shorter hydrogen bond (1.67 Å instead of 1.74 Å in the wild type). The positions of the inhibitor, Glu-386, and the other residues are identical to those in the wild-type active site. If Glu-215 is replaced with an aspartate or an alanine, these residues do not interact with the inhibitor. In the Asp-215

	215	352	386
APA mouse	DGQIRSIATDHE PT DARKSFPCFDEPN---116---T GAMEN WGLVITYRETNLLYDPLLSASSNQQRVASVVA HEL VHQWFGNTVTMDW		
APA human	NGRVKSIATDHE PT DARKSFPCFDEPN---116---T GAMEN WGLITYRETNLLYDPKESASSNQQRVATVVA HEL VHQWFGNIVTMDW		
IRAP rat	SNEKKNFATQ E PLAARSAFPCFDEPA---116---A GAMEN WGLLTFREETLLYDNATSSVADRKLVTKIIA HEL AHQWFGNLVTMQW		
PSA mouse	AGEVRYAAVTQ E ATDPRRAFPCWDEPA---119---A GAMEN WGLVITYRETALLIDPKNSCSSRQWVALVV HEL AHQWFGNLVTMEW		
LTA4H rat	SGKQHPYLF SQ Q AI HCRAILPCQDT-S---115---Y GGMEN PCLTFVTPPTLLAGDKSLs-----NVIA HEL ISHSWTGNLVTNKT		
LTA4H mouse	SGKQHPYLF SQ Q AI HCRAILPCQDTPS---115---Y GGMEN PCLTFVTPPTLLAGDKSLs-----NVIA HEL ISHSWTGNLVTNKT		
LTA4H human	SGKEHPYLF SQ Q AI HCRAILPCQDTPS---115---Y GGMEN PCLTFVTPPTLLAGDKSLs-----NVIA HEL ISHSWTGNLVTNKT		
APB rat	AGKKKPVFYTQ G AVLNRAFFPCFDTPA---110---F GGMEN PCLTFVTPCLLAGDRSLA-----DVII HEL ISHSWFGNLVTNAN		
APN rat	GGNKKVVATTQ Q AADARKSFPCFDEPA---118---A GAMEN WGLVITYRESALVFDQSSSISNKERVVTVIA HEL AHQWFGNLVTVDW		
APN mouse	GDVKKVVATTQ Q AADARKSFPCFDEPA---121---A GAMEN WGLVITYRESSLVFDSQSSSISNKERVVTVIA HEL AHQWFGNLVTVAW		
APN human	GNVRKVVATTQ Q AADARKSFPCFDEPA---122---A GAMEN WGLVITYRENSLLFDPLSSSSISNKERVVTVIA HEL AHQWFGNLVTIEW		

FIGURE 2: Alignment of the mouse APA amino acid sequence with the sequences of other monozinc aminopeptidases. The consensus zinc-binding motif, HEXXH, is in *italics*; the conserved residue glutamate 215 in APA and the homologous residues in other sequences are in **bold type**. The conserved GXMEN motif is also indicated in **bold type**. We show an alignment of the amino acid sequences of mouse and human APA (EC 3.4.11.7), rat insulin-regulated membrane aminopeptidase (IRAP, EC 3.4.11.3), mouse puromycin-sensitive aminopeptidase (PSA, EC 3.4.11.14), rat, mouse, and human leukotriene A4 hydrolase (LTA4H, EC 3.3.2.6), rat aminopeptidase B (APB, EC 3.4.11.6), and rat, mouse, and human aminopeptidase N (APN, EC 3.4.11.2).

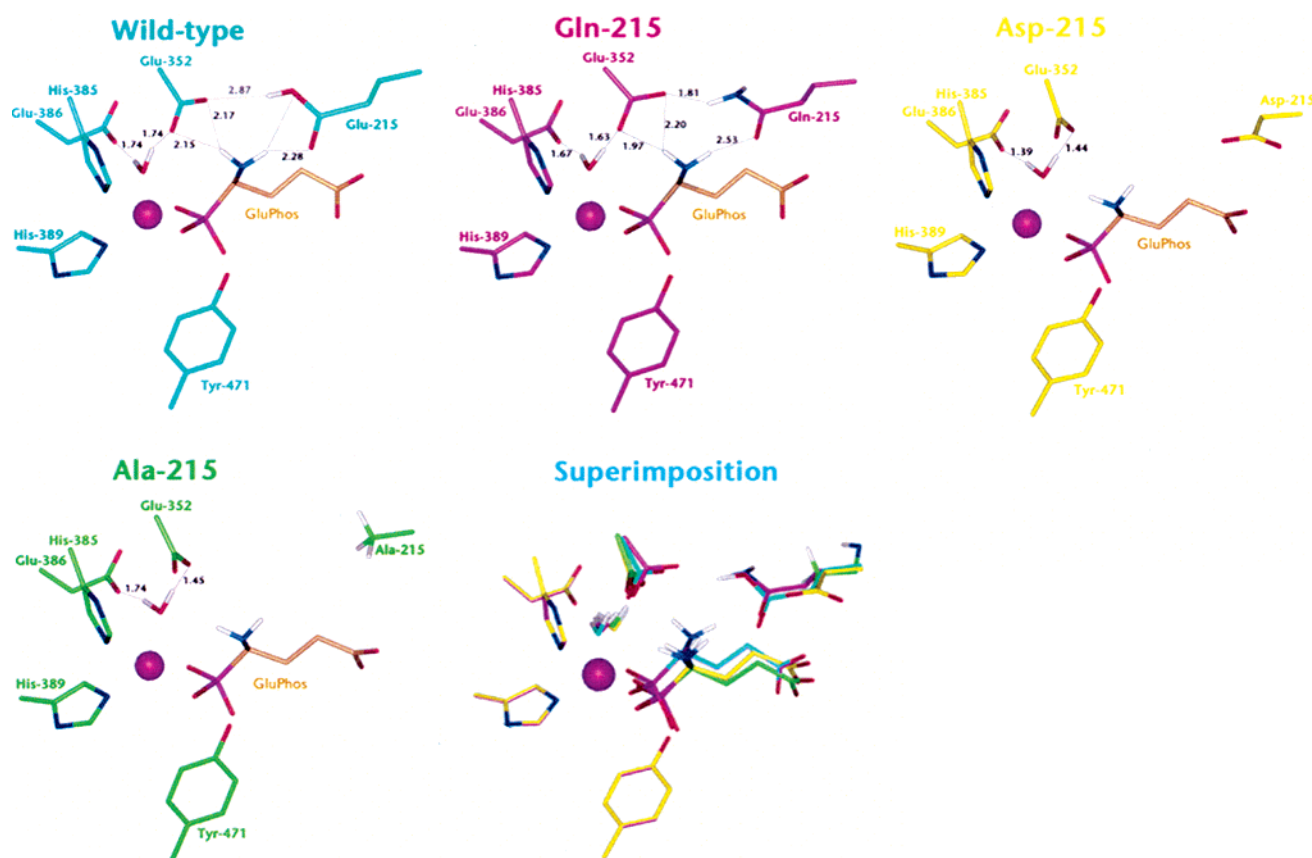


FIGURE 3: Comparison of active site organization in wild-type and mutated APAs. We show the models of the active sites of wild-type APA and the mutated Gln-215, Asp-215, and Ala-215 APA enzymes and the superimposition of these four models. Wild-type residues are colored blue. Gln-215 residues are colored magenta. Asp-215 residues are colored yellow. Ala-215 residues are colored green. The carbon atoms of the inhibitor GluPhos docked in the active sites are colored brown. In the superimposition, the inhibitor is shown in the same color as the active site residues. In all the models, the zinc atom is shown as a purple sphere. The hydrogen bonds are depicted as gray lines. Distances are given in angstroms.

and Ala-215 mutant models, the position of the Glu-352 side chain differs from that in the wild-type active site, and this side chain no longer interacts with the inhibitor. However, Glu-352 still bonds to the water molecule, the position of which also differs from that in the wild-type active site. The position of the inhibitor is also different from that in the wild-type active site. The position of the other constituents of the active site is not affected by the mutation.

Construction, Expression, and Purification of Recombinant His-APAs. In the 3D model of APA, we identified a residue,

Glu-215, that interacts directly with the N-terminal amino group of the inhibitor via two hydrogen bonds involving the oxygens of its carboxyl group. We investigated the function of Glu-215 in mouse APA by replacing this residue with a glutamine, an aspartate, or an alanine by site-directed mutagenesis. We first checked that the mutations did not affect the expression and maturation of the recombinant proteins. Stably transfected CHO cells producing wild-type and mutated His₆-APAs were labeled by incubation with [³⁵S]-methionine/cysteine for 5 h and then lysed in detergent

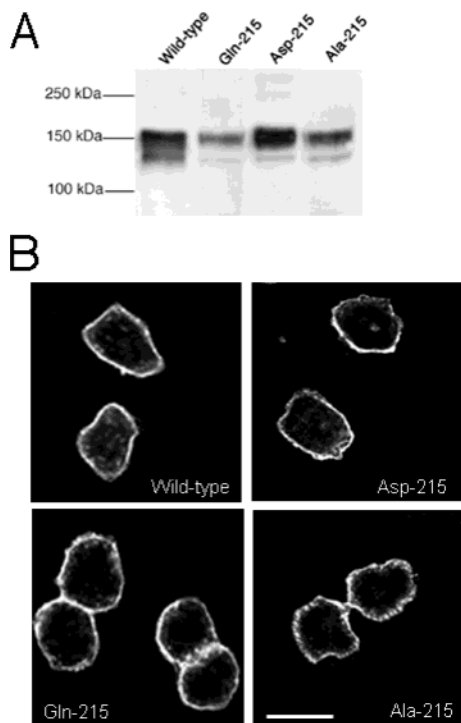


FIGURE 4: Expression and maturation of histidine-tagged wild-type and mutated mouse recombinant APAs. (A) Transfected CHO cells stably expressing wild-type and mutated His₆-APAs were labeled by incubation for 5 h with a [³⁵S]methionine/cysteine mixture. Solubilized cell lysate proteins were immunoprecipitated with a monoclonal anti-His₅ antibody, resolved by 5% SDS–PAGE, and analyzed with a Molecular Imager FX Proplus machine. The following molecular mass markers were used: 250, 150, and 100 kDa. (B) Transfected CHO cells stably expressing wild-type and mutated His₆-APAs were fixed and immunolabeled with a rabbit polyclonal anti-(rat-APA) serum and detected with a cyanin 3-conjugated anti-rabbit antibody. Immunofluorescence was observed by confocal microscopy. The bar is 20 μ m.

buffer, and recombinant His₆-APAs were immunoprecipitated with an anti-His₅ antibody. The immunoprecipitates were subjected to SDS–PAGE, and the gels were analyzed with a Molecular Imager FX Proplus machine (Figure 4A). Wild-type and mutated His₆-APAs displayed two bands, 168 and 140 kDa in size, corresponding to specifically immunoprecipitated proteins. We then investigated the subcellular distribution of wild-type and mutated His₆-APAs in stably transfected CHO cells, by immunofluorescence analysis with a rabbit polyclonal anti-(rat APA) antibody and a cyanin-3-conjugated anti-rabbit secondary antibody. Confocal microscopy analysis of CHO cells producing wild-type His₆-APA or the Gln-215, Asp-215, or Ala-215 mutant showed that APA was located in the plasma membrane (Figure 4B).

Enzymatic Activity of Purified Recombinant His₆-APAs. The enzymatic activities of purified recombinant His₆-APAs were analyzed by determining the catalytic constants (K_m and k_{cat}) under standard conditions, in the presence of 4 mM Ca²⁺, using GluNA as a substrate. The results are summarized in Table 1. The replacement of Glu-215 with a glutamine led to a slight but not significant effect on substrate hydrolysis. Kinetic studies showed that this slight difference was due to increases in K_m (5.5 times) and k_{cat} (6.8 times), resulting in a 1.25-fold increase in the k_{cat}/K_m ratio for Gln-215.

The replacement of Glu-215 with an aspartate or an alanine resulted in rates of GluNA hydrolysis significantly lower than

Table 1: Kinetic Parameters for Wild-Type and Mutated APAs in the Presence of 4 mM Ca²⁺

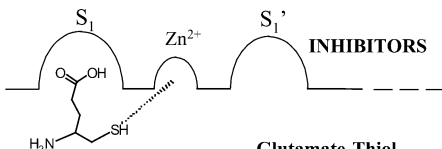
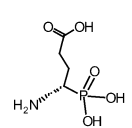
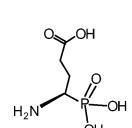
enzyme	K_m^a (mM)	k_{cat}^a (s ⁻¹)	k_{cat}/K_m (mM ⁻¹ s ⁻¹)
wild-type	0.16 \pm 0.01	270 \pm 20	1688
Gln-215	0.87 \pm 0.06	1800 \pm 100	2070
Asp-215	1.50 \pm 0.30	19 \pm 4	12
Ala-215	2.80 \pm 0.40	48 \pm 5	17

^a K_m and k_{cat} values are the means \pm the standard error of the mean of at least three separate experiments with duplicate determinations.

that observed for the wild-type enzyme. The K_m values of the Asp-215 and Ala-215 mutants were 9.5 and 17.5 times higher than that of the wild-type APA, respectively, whereas the corresponding k_{cat} values were lower than that of the wild-type APA by factors of 14 and 6, respectively. This resulted in k_{cat}/K_m ratios lower than those of the wild-type APA by a factor of 141 for Asp-215 and by a factor of 100 for Ala-215.

Potency of Various Classes of the Compound To Inhibit Purified Recombinant His₆-APAs. We further characterized the role of Glu-215 in inhibitor binding by evaluating the potential of two classes of compounds to inhibit the enzyme. These inhibitors differed in zinc-chelating group and structure: GluSH, which binds to the S1 subsite and possesses a strong zinc-chelating group, and the two isomers (L and D) of GluPhos, which differ in the orientation of their α -amino group. L-GluPhos, a pseudoanalogue of the transition state, was shown to be a potent APA inhibitor (K_i = 0.045 μ M), with inhibition mediated by one of the phosphoryl oxygens of this molecule that interacts with the zinc ion, and another with the phenolic hydroxyl group of Tyr-471 (11). We evaluated the extent to which these compounds inhibited GluNA (0.5 mM) hydrolysis in the presence of a supramaximal concentration of Ca²⁺ (4 mM). The results are summarized in Table 2. The substrate analogue D,L-GluSH inhibited all three mutant enzymes less strongly than the wild-type enzyme, by factors of 2 for Gln-215, 50 for Asp-215, and 71 for Ala-215 (wild-type enzyme K_i = 0.147 μ M). L-GluPhos also inhibited the three mutant enzymes less strongly than the wild-type enzyme, by factors of 4.6 for Gln-215, 267 for Asp-215, and 467 for Ala-215 (wild-type enzyme K_i = 0.045 μ M). In contrast, the decrease in the inhibitory potency of D-GluPhos was greater for Gln-215 (factor of 8.4) than for Asp-215 (factor of 3) and Ala-215 (factor of 5.9) compared to that of the wild-type enzyme (K_i = 1.91 μ M). We assessed the importance of the free amino group for the binding of inhibitors to APA by comparing the extent to which L- and D-GluPhos were able to inhibit recombinant His₆-APAs (Figure 5). L-GluPhos was found to be 42 times more efficient than D-GluPhos at inhibiting wild-type APA-induced GluNA hydrolysis. For the Gln-215 mutant, a similar difference (factor of 63) was observed in the efficiency of the two isomers for the inhibition of GluNA hydrolysis. For the Asp-215 and Ala-215 mutant enzymes, the two inhibitors differed in potency by a factor of only 0.5. To further determine the influence of the free amino group of the inhibitors on their ability to inhibit recombinant His₆-APAs, we used two compounds which displayed a zinc binding phosphonic acid group, together with or without a free amine group (GlyPhos and methylPhos, respectively). Even if these molecules are weak APA inhibitors (K_i = 85 μ M for GlyPhos and 787 μ M for methylPhos), they enable

Table 2: K_i Values (μM) for Several Inhibitors with Wild-Type (WT) and Mutated APAs^a

	WT	Gln-215	Asp-215	Ala-215
 <p>Glutamate-Thiol</p>	0.147 ± 0.008	0.340 ± 0.006***	7.2 ± 0.8***	10 ± 1 ***
 <p>L-Glutamate phosphonic acid</p>	0.045 ± 0.002	0.26 ± 0.05*	12.0 ± 0.6***	21 ± 3**
 <p>D-Glutamate phosphonic acid</p>	1.9 ± 0.4^^	16 ± 1***^^	5 ± 1*	11 ± 1***

^a K_i values are the means ± the standard error of the mean of at least three different experiments with duplicate determinations. One asterisk means $P < 0.05$. Two asterisks mean $P < 0.01$. Three asterisks mean $P < 0.001$ (mutated APAs vs the wild type). Two ^ symbols mean $P < 0.01$. Three ^ symbols mean $P < 0.001$ (D-glutamate phosphonic acid vs L-glutamate phosphonic acid).

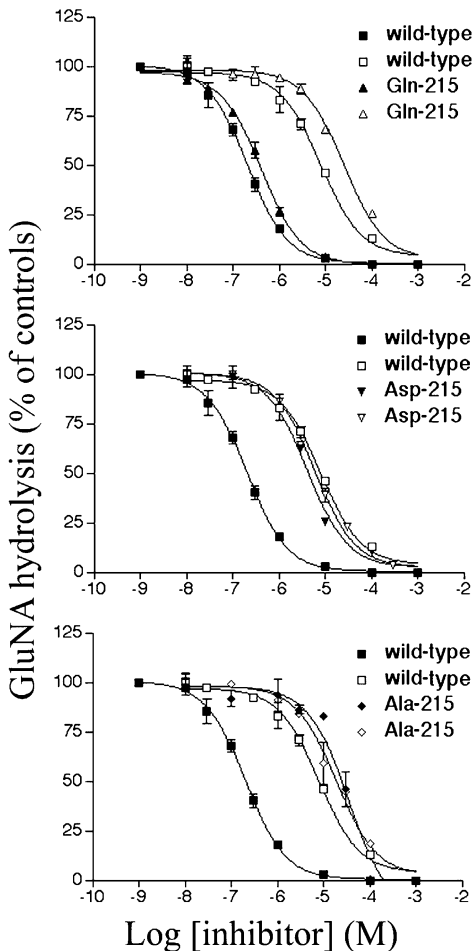


FIGURE 5: Effect of L- and D-GluPhos on the enzymatic activity of wild-type and mutated His₆-APAs. APA activities were evaluated by measuring the rate of hydrolysis of 0.5 mM GluNA in the presence of 4 mM CaCl₂, in the presence or absence of various concentrations of L- and D-GluPhos. Filled symbols depict APA activity inhibited by L-GluPhos, and empty symbols depict APA activity inhibited by D-GluPhos. Each point represents the mean ± the standard error of the mean of three independent experiments with duplicate determinations.

us to study the interactions of recombinant enzymes with the N-terminal amine of the inhibitors without the influence

of the side chain. GlyPhos was found to be 10 times more efficient than methylPhos at inhibiting wild-type APA. A factor of 10 was also observed between the efficiency of the two inhibitors for the inhibition of the Gln-215 mutant. By contrast, for the Asp-215 mutant, the two inhibitors differed in potency by a factor of only 2. These results are in agreement with those obtained with the two isomers of GluPhos.

DISCUSSION

We recently generated a three-dimensional model of the mouse APA ectodomain, using the X-ray crystal structure of LTA4H as a template (16). We also modeled the enzyme with the specific and selective APA inhibitor GluPhos, an analogue of the transition state, docked into the active site. We observed that Glu-352, which is located within the 349-GXMEN-352 motif, and Glu-215 were present in the active site, near the zinc atom, together with the catalytic glutamate Glu-386 and the zinc ligands. Furthermore, both Glu-352 and Glu-215 interact with GluPhos via hydrogen bonds between their acidic side chains and the free amino group of the inhibitor. Similarly, the crystal structure of LTA4H showed hydrogen bonds between residues Glu-271 and Gln-136 and the N-termini of bestatin (15) and of two competitive tight binding inhibitors, a thioamine and a hydroxamic acid (29). Previous mutagenic studies on the strictly conserved glutamate of the consensus GXMEN sequence, in APA (Glu-352) (12), APN (Glu-350) (18), oxytocinase (Glu-431) (30), and LTA4H (Glu-271) (19), all revealed that this residue is part of a binding site for the substrate N-terminus, contributing to the exopeptidase specificity of these enzymes through interactions with the free N-terminal amine of the substrate.

Alignment of the sequence of mouse APA with those of other monozinc aminopeptidases in the region located upstream from the HEXXH zinc binding motif showed that Glu-215 (in APA) is not a strictly conserved residue. The aligned residues are either glutamates or glutamines. However, glutamate and glutamine each have a carbonyl group in the same position on their side chains, enabling them to interact with the N-terminal amino group of the substrate. This functional conservation is consistent with the hypothesis

that Glu-215 is involved in substrate binding, as shown by the 3D model of wild-type APA.

The functional role of Glu-215 was investigated by replacing this residue by site-directed mutagenesis with an aspartate, which resulted in retraction of the carboxylate group, an alanine, which eliminated the carboxylate group, or a glutamine, which maintained the presence of an amide carbonyl group at the same position.

The replacement of Glu-215 with an aspartate or an alanine led to a strong decrease in the rate of hydrolysis of the synthetic substrate GluNA. Kinetic studies showed that the K_m values of Asp-215 and Ala-215 were 10 and 18 times higher, respectively, than that of the wild-type enzyme, indicating that Glu-215 is involved in substrate binding. The k_{cat} values of Asp-215 and Ala-215 were lower than that of the wild-type enzyme, by factors of 14 and 6, respectively, reducing the efficiency of hydrolysis of the two mutant enzymes by factors of 141 and 100, respectively, indicating that Glu-215 is also involved in the catalytic process of APA. The insertion of these mutations into the 3D model demonstrated that aspartate or alanine residues in position 215 do not interact with the N-terminal part of the inhibitor, accounting for the major decrease in the affinity of the mutated enzymes for the substrate. In addition, the mutations lead to a change in the position of the inhibitor GluPhos in the active site such that it does not interact with Glu-352. The difference in the positioning of this transition state analogue with respect to wild-type APA may account for the lower k_{cat} values obtained for these mutant proteins. In contrast, the replacement of Glu-215 with a glutamine (Gln-215) had no significant effect on GluNA hydrolysis, if anything slightly increasing it. This slight increase was due to a decrease in the affinity of the mutated enzyme for the substrate (by a factor of 5.5), together with a higher rate of substrate hydrolysis (6.8 times higher). The smaller decrease in the affinity of the Gln-215 mutant for the substrate than in the affinities of the other mutant proteins suggests that an interaction persists between the Gln-215 side chain and the substrate. Indeed, in the 3D model of the Gln-215 mutant, a hydrogen bond remains between the carbonyl group of Gln-215 and the free amine of the inhibitor as shown for LTA4H (15), possibly accounting for the slight decrease in affinity of the Gln-215 mutant enzyme with respect to that of the wild-type enzyme. Interestingly, the NH_2 group of the amide group of the Gln-215 side chain establishes a new additional interaction by hydrogen bonding with the carboxyl group of Glu-352. This interaction stabilizes Glu-352 in a position optimal for polarization of the catalytic water molecule, thereby strengthening nucleophilic attack on the scissile peptide bond. This in turn results in an increase in the rate of substrate cleavage, consistent with the higher rate of substrate hydrolysis observed for the Gln-215 mutant.

We further characterized the role of Glu-215 in the active site of APA by evaluating the extent to which various classes of inhibitors inhibited the wild-type and mutated enzymes. The inhibitors studied were (i) a β -aminothiol derivative, the inhibitor GluSH, which interacts with the amine binding site, the S1 subsite, and the zinc ion via its chelating thiol group, and (ii) an α -amino phosphonate inhibitor, GluPhos, which interacts with the amine binding site, the S1 subsite, with Tyr-471 involved in transition state stabilization, and with the zinc ion via its phosphoryl oxygens. We used the L and

D conformations of GluPhos, which differ in terms of the orientation of their α -amino groups.

Mutating Glu-215 to either aspartate or alanine greatly reduced the affinity of the mutant enzyme for GluSH (by a factor of 50 or 71, respectively) and for L-GluPhos (by a factor of 276 or 467, respectively). The much lower levels of inhibition observed with the mutant proteins than with the wild-type protein suggest that there is an interaction between the Glu-215 side chain and these two inhibitors.

To demonstrate that Glu-215 interacted with the free α -amino group of the inhibitors, we compared the capacity of L- and D-GluPhos to inhibit wild-type and mutated APA enzymes. For wild-type APA, L- and D-GluPhos differed in inhibitory potency by a factor of 42. For Gln-215, the two inhibitors showed a similar difference in inhibitory potency (a factor of 63). In contrast, for Ala-215 and Asp-215, the two inhibitors differed in potency by a factor of only 0.5. The large difference in the affinity of wild-type APA for the L and D conformations of the inhibitor results from differences in the positioning of the free N-terminal amino group of the inhibitor in the active site of APA. The much smaller difference in the affinity of Ala-215 and Asp-215 for the two conformations suggests that these mutations abolish the binding of the free N-terminal part of the inhibitor to the mutated residues. As the amplitudes of the difference in the affinity of wild-type and Gln-215 for L- and D-GluPhos are similar, Gln-215 would also appear to be hydrogen-bonded to the amine moiety of the inhibitor, confirming the interaction predicted by the 3D model. To further strengthen this conclusion, the inhibitory potencies of two other inhibitors, GlyPhos and methylPhos, lacking the acidic lateral chain and displaying a zinc binding phosphonic acid group with or without a free amine group were evaluated on wild-type and mutated APAs. Despite the weak affinity of these compounds for APA because of the absence of the lateral chain, a difference of a factor of 10 was observed between the K_i values of both compounds for wild-type APA and the Gln-215 mutant, due to the absence of the free amino group in methylPhos. In contrast, a difference of a factor of only 2 was noticed for the Asp-215 mutant, confirming the interaction of the amine moiety of the inhibitor with Glu-215. Furthermore, the Asp-215 and Ala-215 mutations produce larger increases in the K_i values of L-GluPhos, which behaves as a transition state analogue, than in those of GluSH, which is consistent with the observed decreases in the k_{cat} values of the corresponding mutated enzymes. These data indicate that Glu-215 is involved in substrate binding and also, indirectly, in the catalytic process, ensuring the correct positioning of the substrate in the active site. Data from modeling let us propose that the interaction between Glu-215 and the substrate would lead to a catalytically competent position of Glu-352. This could account for the influence of the Asp-215 and Ala-215 mutations on the catalytic process.

Interestingly, the counterpart of Glu-215 in LTA4H, Gln-136, was shown, in the crystal structure of the enzyme, to interact with the α -amino group of various cocrystallized inhibitors, suggesting that this residue is part of the substrate N-terminal binding site of the enzyme (15, 29). However, site-directed mutagenesis of Gln-136 was inconclusive concerning the role of this residue (19), possibly because LTA4H is not strictly an aminopeptidase.

In conclusion, in this study, on the basis of the 3D model of APA and the results of site-directed mutagenesis, we suggest that the exopeptidase specificity of APA is determined by Glu-215 and Glu-352, which together constitute the binding site for the N-terminus of substrates and inhibitors. This study confirms that the 3D model of APA constitutes a useful tool for investigating the organization of the APA active site, and to gain new insight into its catalytic mechanism.

ACKNOWLEDGMENT

We thank Dr. S. Wilk and Dr. D. Healy for providing the APA antiserum and Dr. B. Lejczak for the gift of the inhibitor GluPhos.

REFERENCES

- Nagatsu, I., Nagatsu, T., Yamamoto, T., Glenner, G. G., and Mehl, J. W. (1970) *Biochim. Biophys. Acta* 198, 255–270.
- Wilk, S., and Healy, D. (1993) *Adv. Neuroimmunol.* 3, 195–207.
- Lodja, Z., and Gossrau, R. (1980) *Histochemistry* 67, 267–290.
- Zini, S., Masdehors, P., Lenkei, Z., Fournie-Zaluski, M. C., Roques, B. P., Corvol, P., and Llorens-Cortes, C. (1997) *Neuroscience* 78, 1187–1193.
- Chauvel, E. N., Llorens-Cortès, C., Coric, P., Wilk, S., Roques, B., and Fournié-Zaluski, M. C. (1994) *J. Med. Chem.* 37, 2950–2956.
- Zini, S., Fournié-Zaluski, M. C., Chauvel, E., Roques, B. P., Corvol, P., and Llorens-Cortès, C. (1996) *Proc. Natl. Acad. Sci. U.S.A.* 93, 11968–11973.
- Reaux, A., de Mota, N., Zini, S., Cadel, S., Fournié-Zaluski, M., Roques, B. P., Corvol, P., and Llorens-Cortes, C. (1999) *Neuroendocrinology* 69 (5), 370–376.
- Reaux, A., Fournie-Zaluski, M. C., and Llorens-Cortes, C. (2001) *Trends Endocrinol. Metab.* 12 (4), 157–162.
- Wang, J. Y., and Cooper, M. D. (1993) *Proc. Natl. Acad. Sci. U.S.A.* 90, 1222–1226.
- Vazeux, G., Wang, J., Corvol, P., and Llorens-Cortès, C. (1996) *J. Biol. Chem.* 271, 9069–9074.
- Vazeux, G., Iturrioz, X., Corvol, P., and Llorens-Cortes, C. (1997) *Biochem. J.* 327, 883–889.
- Vazeux, G., Iturrioz, X., Corvol, P., and Llorens-Cortes, C. (1998) *Biochem. J.* 334 (Part 2), 407–413.
- Iturrioz, X., Vazeux, G., Celerier, J., Corvol, P., and Llorens-Cortes, C. (2000) *Biochemistry* 39 (11), 3061–3068.
- Iturrioz, X., Rozenfeld, R., Michaud, A., Corvol, P., and Llorens-Cortes, C. (2001) *Biochemistry* 40 (48), 14440–14448.
- Thunnissen, M. M., Nordlund, P., and Haeggstrom, J. Z. (2001) *Nat. Struct. Biol.* 8 (2), 131–135.
- Rozenfeld, R., Iturrioz, X., Maigret, B., and Llorens-Cortes, C. (2002) *J. Biol. Chem.* 277 (32), 29242–29252.
- Lejczak, B., Choszczak, M. P. D., and Kafarski, P. (1993) *J. Enzyme Inhib.* 7, 97–103.
- Luciani, N., Marie-Claire, C., Ruffet, E., Beaumont, A., Roques, B. P., and Fournie-Zaluski, M. C. (1998) *Biochemistry* 37, 686–692.
- Rudberg, P. C., Tholander, F., Thunnissen, M. M., and Haeggstrom, J. Z. (2002) *J. Biol. Chem.* 277 (2), 1398–1404.
- Dewar, M. J. S., Zebisch, E. G., Healy, E. F., and Stewart, J. J. P. (1985) *J. Am. Chem. Soc.* 107 (13), 3902–3909.
- Liljefors, T., and Norrby, P. (1997) *J. Am. Chem. Soc.* 119 (5), 1052–1058.
- Herlitze, S., and Koenen, M. (1990) *Gene* 91, 143–147.
- Wu, Q., Lahti, J. M., Air, G. M., Burrows, P. D., and Cooper, M. D. (1990) *Proc. Natl. Acad. Sci. U.S.A.* 87, 993–997.
- Laemmli, U. K. (1970) *Nature* 227, 680–685.
- Bradford, M. M. (1976) *Anal. Biochem.* 72, 248–254.
- Song, L., Ye, M., Troyanovskaya, M., Wilk, E., Wilk, S., and Healy, D. P. (1994) *Am. J. Physiol.* 267, F546–F557.
- Chauvel, E. N., Coric, P., Llorens-Cortès, C., Wilk, S., Roques, B. P., and Fournié-Zaluski, M. C. (1994) *J. Med. Chem.* 37, 1339–1346.
- Wilk, S., and Thurston, L. S. (1990) *Neuropeptides* 16, 163–168.
- Thunnissen, M. M., Andersson, B., Samuelsson, B., Wong, C. H., and Haeggstrom, J. Z. (2002) *FASEB J.* 16 (12), 1648–1650.
- Laustsen, P. G., Vang, S., and Kristensen, T. (2001) *Eur. J. Biochem.* 268 (1), 98–104.

BI034358U